Biochemical, Mössbauer, and EPR Studies of the Diiron Cluster of Phenol Hydroxylase from *Pseudomonas* sp. Strain CF 600[†]

Elisabeth Cadieux,[‡] Vladislav Vrajmasu,[§] Catalina Achim,[§] Justin Powlowski,*[,‡] and Eckard Münck*[,§]

Department of Chemistry and Biochemistry, Concordia University, 1455 de Maisonneuve Boulevard West, Montreal, Quebec, Canada, H3G 1M8, and Department of Chemistry, Carnegie Mellon University, 4400 Fifth Avenue, Pittsburgh, Pennsylvania 15213

Received March 29, 2002; Revised Manuscript Received June 28, 2002

ABSTRACT: Phenol hydroxylase of *Pseudomonas* sp. strain CF600 comprises three components: DmpP is an FAD- and [2Fe-2S]-containing reductase; DmpM is a cofactorless activator protein; and DmpLNO is the oxygenase. Single turnover experiments established that DmpLNO contains the active site, but requires DmpM for efficient turnover: the steady-state turnover rate reaches a maximum at 1.5 DmpM:1 DmpLNO. Chemical cross-linking experiments showed that DmpM interacts with the large subunit of the DmpLNO oxygenase complex. Mössbauer studies revealed that the active site of the oxygenase can accommodate two types of diiron clusters, each of these cluster types having two equivalent sites. Cluster form I, representing typically around 85% of total Fe, has $\Delta E_Q = 1.73$ mm/s and $\delta = 0.54$ mm/s, while cluster II exhibits $\Delta E_Q = 0.79$ mm/s and $\delta = 0.48$ mm/s. Studies in strong applied magnetic fields suggest that the two iron sites of cluster I are bridged by an oxo group while sites in cluster II appear to be hydroxo-bridged. Reduction of the samples with dithionite yields the diferrous forms of the clusters. Air oxidation of the reduced samples leads to an increase of the cluster II fraction, accompanied by a corresponding decrease in catalytic activity. The reduced oxygenase samples exhibit at X-band an integer spin EPR signal centered, in parallel mode, at $g = 16.6$. Quantitative analysis showed that 19% of the clusters contribute to the EPR signal, suggesting that cluster II is the EPR-active species. Incubation with dithiothreitol (DTT) inactivated the oxygenase by a mechanism apparently involving H_2O_2 generation. In addition, Mössbauer studies of DTT-inactivated enzyme showed that all ferric iron belonged to one diamagnetic diferric cluster with parameters that indicate that DTT coordinates to the cluster.

The versatility of aerobic microorganisms in degrading aromatic compounds is reflected in the wide array of oxygenases that are used to initiate metabolic processing of these molecules. Destabilization of the aromatic ring is achieved by enzymatic insertion of one or more oxygen atoms, allowing further attack by ring-cleavage dioxygenases. The resulting nonaromatic products are transformed stepwise into central metabolites such as pyruvate and acetyl-CoA (*1*). The specificity and efficiency of the ring-hydroxylating enzymes are therefore important in controlling the entry of potential growth substrates into metabolism.

While all oxygen-activating enzymes require redox-active metals or prosthetic groups, two broad categories of aromatic ring hydroxylases may be distinguished: those that consist of a single polypeptide and those that are comprised of more than one polypeptide component. The single polypeptide oxygenases characterized to date contain FAD[1] as the sole redox-active element responsible for insertion of one oxygen atom from O_2 into the substrate, and reduction of the other oxygen atom to H_2O using electrons from NAD(P)H (reviewed in *2*). All these enzymes act on monohydroxylated aromatics such as *o*- or *p*-hydroxybenzoate and phenol, or on aromatic amines. On the other hand, the chemically more difficult oxygenation of aromatic rings *lacking* electron-donating substituents (e.g., toluene, naphthalene, and biphenyl) is carried out by microbial oxygenases that contain non-heme iron cofactors (reviewed in *3*−*5*). For these enzymes, one or more auxiliary polypeptides are required to transfer electrons into the oxygenase active site. Non-heme iron prosthetic groups are also found in microbial oxygenases used to initiate degradation of various alkanes and alkenes (*5*−*7*).

[†] This work was supported by a research grant from the Natural Sciences and Engineering Research Council of Canada (J.P.) and by NIH Grant GM 22701 (E.M.). E.C. was a recipient of a doctoral scholarship from Fonds pour la Formation de Chercheurs et l'Aide à la Recherche.

* To whom correspondence should be addressed. J.P.: Phone (514)-848-8727; Fax (514)-848-2868; E-mail powlow@vax2.concordia.ca. E.M.: Phone (412)-268-5058; Fax (412)-268-1061; E-mail em40@andrew.cmu.edu.

[‡] Concordia University.

[§] Carnegie Mellon University.

[1] Abbreviations: ACP, acyl carrier protein; BCA, bicinchoninic acid; DEAE, diethylaminoethyl; DTT, dithiothreitol; EDC, 1-ethyl-3-(3-dimethylaminopropyl)carbodiimide hydrochloride; EDTA, ethylenediaminetetraacetic acid; EPR, electron paramagnetic resonance; FAD, flavin adenine dinucleotide; HEPES, *N*-(2-hydroxyethyl)piperazine-*N*′-2-ethanesulfonic acid; MMOB, activator protein of methane monooxygenase; MMOH, oxygenase component of methane monooxygenase; MOPS, 3-(*N*-morpholino)propanesulfonic acid; NAD(P)H, dihydronicotinamide adenine dinucleotide (phosphate); NHS, *N*-hydroxysuccinimide; SDS, sodium dodecyl sulfate; TG, Tris-HCl glycerol; Tris, tris(hydroxymethyl)aminomethane; UV/Vis, ultraviolet/visible.

10.1021/bi025901u CCC: $22.00
Published on Web 08/02/2002

A rather unique situation exists in the phenol degrader *Pseudomonas sp.* strain CF600, which uses a multicomponent oxygenase for this activated aromatic compound (*8*). Sequence comparisons and biochemical studies indicate that the polypeptide components of this enzyme are related to the components of methane monooxygenase, which comprises a binuclear iron center containing hexameric $(\alpha\beta\gamma)_2$ oxygenase, a reductase containing an FAD/[2Fe-2S] center, and a small activator protein lacking any redox cofactors (reviewed in *5*). However, other than the putative iron center ligands, the overall level of similarity between the phenol hydroxylase components and those of methane monooxygenase is rather low (*8*). Sequence comparisons also indicate similarities with polypeptides involved in oxygenation of toluene at the 2- and 4-positions, as well as with phenol hydroxylase components from other bacterial strains (*8*, *9*). Therefore, the study of the multicomponent phenol hydroxylase is of interest in that it is widely used by various bacterial strains, and in that it is a representative of a growing class of oxygenases of which only methane monooxygenase has been extensively characterized.

We have previously reported the purification and characterization of the reductase (DmpP) and activator (DmpM) components of this multicomponent enzyme, as well as DmpK, which appears to be involved in the assembly of the oxygenase (*10*−*12*). In this paper, purification of the oxygenase is reported, and we show that its active site contains a binuclear iron cluster similar to those reported for other diiron proteins.

EXPERIMENTAL PROCEDURES

Chemicals and Materials. Fast-Flow DEAE-Sepharose, Phenyl-Sepharose High Performance, and Sephacryl S-300HR were purchased from Amersham-Pharmacia Biotech (Montreal, Quebec, Canada). ^{57}Fe was obtained from Icon Services Inc. (Summit, NJ). The BCA Protein assay kit and the cross-linkers EDC and sulfo-NHS were purchased from Pierce (Rockford, IL). All other chemicals were reagent grade or better.

Bacterial Growth. Cultures of *Pseudomonas* sp. strain CF600 were grown in minimal medium with phenol as previously described (*11*) except that the pH of the growth medium was maintained at 7.0−7.5 by the addition of NaOH rather than NH_4OH. Frozen cell paste was thawed in 50 mM Tris-HCl, pH 8, containing 10% glycerol and 200 μM ferrous ammonium sulfate (2 mL of buffer/g of cell paste). A spatula tip of deoxyribonuclease was added, and after 5 min, the cell suspension was sonicated for 10 bursts of 15 s each, in 40 mL batches cooled by an ice/saltwater bath. The temperature of the cell suspension during sonication was not allowed to rise above 10 °C. After centrifugation at 70400*g* for 60 min, the supernatant ("crude extract") was collected and used for further purification.

Purification of the Oxygenase (DmpLNO). Crude extract was loaded onto a Fast-Flow DEAE-Sepharose column (30 × 2.6 cm) previously equilibrated with 50 mM Tris-HCl, pH 8, containing 10% glycerol ("TG buffer"). The column was then washed (1 mL/min) with 75 mM NaCl in TG buffer (250 mL), and the oxygenase (DmpLNO) was eluted by applying a 75−275 mM NaCl gradient in TG buffer (1000 mL). Fractions (12 mL) containing oxygenase activity eluted approximately in the middle of the gradient. These fractions were combined and brought to 65% saturation with ammonium sulfate. After 30 min, the precipitate was collected by centrifugation at 15300*g* for 30 min. The pellet was redissolved in TG buffer (30 mL), and the solution was clarified by centrifugation at 3800*g* for 20 min before loading it onto the next column.

The preparation was loaded onto a Phenyl-Sepharose High Performance column (36 × 2.6 cm) previously equilibrated with TG buffer containing 0.15 M NaCl. The column was washed (1.5 mL/min) with the same buffer until the eluate was no longer yellow. A second wash with TG buffer only was applied until the absorbance at 280 nm dropped below 0.2. The buffer was then changed to 5 mM Tris-HCl, pH 8.0, containing 10% glycerol, whereupon the oxygenase component eluted. Fractions (12 mL) containing oxygenase activity were combined and concentrated by ultrafiltration with an Amicon YM30 membrane before proceeding to the next step.

The concentrated sample then was loaded (1 mL/min) onto a Sephacryl S-300HR gel filtration column (78 × 2.6 cm) equilibrated with TG buffer, and the oxygenase was eluted with TG buffer. Fractions (12 mL) were collected, and assayed for activity.

Active fractions eluting from the gel filtration column were combined and loaded (4 mL/min) onto a Fast-Flow DEAE-Sepharose column (18 × 1.6 cm), previously equilibrated with TG buffer containing 75 mM NaCl. Unbound protein was eluted with the same buffer (120 mL) before starting a 75−200 mM NaCl gradient in TG buffer (500 mL); 5 mL fractions were collected. The oxygenase eluted near the end of the gradient. Fractions with the highest specific activity were combined and concentrated by ultrafiltration using an Amicon YM 30 membrane. Aliquots of the concentrated oxygenase were stored at −80 °C.

Analytical Ultracentrifugation. Purified oxygenase was diluted to 0.32−1 mg/mL with 50 mM Tris-HCl, pH 8.0, in a volume of 500 μL and dialyzed against the same buffer for 1 h. Some samples also contained 0.1 M NaCl. Sedimentation velocity experiments were performed at 20 °C using a Beckman Coulter XL-A analytical ultracentrifuge with an An-60Ti rotor at 28 000 rpm. Data processing was done with DCDT Plus software (*13*).

Preparation of ^{57}Fe-Labeled Oxygenase for Mössbauer Spectroscopy. A ^{57}Fe metal chip (∼15 mg) was placed in a glass test tube and was dissolved over several days in concentrated HCl (0.32 mL) maintained at 60 °C. ^{57}Fe (13 mg) was added as $FeCl_3$ to sterile M9 medium (16 L) in place of unlabeled iron (*11*): this medium was then used for growth of *Pseudomonas* sp. strain CF600 on phenol as described above. Purification of the oxygenase component from these cultures was carried out essentially as described above except that $^{57}FeCl_3$ (200 μM) and ascorbate (2 mM) were added to the cell suspension in place of ferrous ammonium sulfate. After the last purification step, the oxygenase was concentrated using a Centricon YM30 device and then diluted with TG buffer to a protein concentration of between 83 and 116 mg/mL. Purified, concentrated samples (300 μL) were transferred to Mössbauer cups and frozen rapidly in liquid nitrogen.

For the reduction/reoxidation experiments, the Mössbauer cup containing ^{57}Fe-enriched protein was placed into a

Schlenk line, and at least six pump/refill cycles were performed while the sample was still frozen. After the sample was thawed, 45 μL of a 3 mM dithionite solution and 35 μL of 1 mM methyl viologen were added with a syringe through a single septum, and the sample was stirred gently for ca. 20 min with the syringe needle in the Schlenk line before freezing the sample with liquid nitrogen. Once frozen, the sample was removed from the Schlenk line. After performing the Mössbauer experiments of the reduced protein, the sample was thawed in air, transferred into a microfuge tube, gently aerated for ca. 20 min by tilting the tube, transferred back into the Mössbauer cup, and then refrozen. This cycle was repeated twice.

Preparation of DTT-Inactivated Oxygenase for Mössbauer Spectroscopy. A sample of ^{57}Fe-containing oxygenase was prepared as described above. DTT (75 mM) was added to the purified oxygenase (1 mM) and incubated at 4 °C under aerobic conditions in TG buffer for a few days until oxygenase activity was completely lost. The DTT-inactivated sample was transferred to a Mössbauer sample holder and frozen in liquid nitrogen. After Mössbauer analysis, the sample was thawed and dialyzed against 1 L of TG buffer for 2 h. The buffer was changed to fresh TG and dialyzed for an additional 2 h before being refrozen for additional Mössbauer analysis.

Analytical Methods. Protein concentration was estimated using the BCA assay according to the instructions given by the manufacturer (Pierce) for the 60 °C protocol, with bovine serum albumin as the standard; additives that interfere in this assay were first removed using a modified procedure (*14*). Where noted, protein concentrations were also estimated using the spectrophotometric method of Gill and von Hippel (*15*). Iron concentrations were estimated using Ferrozine after removing the protein by trichloroacetic acid precipitation (*16*). SDS−polyacrylamide gel electrophoresis was performed either on 10−20% gradient gels (BioRad) according to established procedures (*17*) or on gels using the Tricine buffer system (*18*).

Enzyme activity was quantitated using a coupled assay for the product, catechol, essentially as described previously (*12*). Concentrations of the hydroxylase components were as follows: DmpP, 0.78 μM; DmpM, 0.24 μM; DmpLNO, 0.18 μM. One unit of activity is defined as the amount of enzyme catalyzing formation of 1 μmol of product/min under these conditions.

UV/Vis spectra were obtained by using Philips PU7415 or Varian Cary Bio50 recording spectrophotometers.

EPR spectra of reduced phenol hydroxylase were recorded at X-band using a Bruker 300 spectrometer equipped with an Oxford ESR 910 cryostat for low-temperature studies and a Bruker bimodal cavity for generating microwave fields parallel and transverse to the static field. The Oxford thermocouple temperature was calibrated using a carbonglass resistor probe (CGR 1, Lake Shore Cryotronics). For determination of the spin concentration, the system was calibrated against copper−EDTA for which the copper concentration was determined by plasma emission spectroscopy. The spectra were analyzed by using a software package written by Dr. M. P. Hendrich at Carnegie Mellon University.

Mössbauer spectra were recorded with constant-acceleration spectrometers, using cryostats that allowed the sample temperature to be varied between 1.5 and 300 K in external magnetic fields up to 8.0 T. The spectra were analyzed using the WMOSS software package (WEB Research, Edina, MN). Isomer shifts are quoted relative to Fe metal at room temperature.

Single Turnover Experiments. Single turnover experiments were carried out in a modified anaerobic quartz cuvette (Hellma) fitted with a gastight syringe via a ground glass joint. The cuvette was loaded in an anaerobic glovebox with phenol hydroxylase (8.9 μM $\alpha\beta\gamma$) and methyl viologen (1 μM) in 50 mM Tris-HCl, pH 7.45, in a total volume of 2 mL. Phenol (12.5 μL of a 0.25 M solution) was contained in a sidearm. The oxygenase was titrated with sodium dithionite solution (~2.9 mM) which was prepared in 50 mM HEPES, pH 8.0, and standardized by titrating into 0.25 mM potassium ferricyanide. Reduction was monitored by the decrease in absorbance at 350 nm (see Figure 5), and was considered to be complete upon the appearance of the reduced methyl viologen peak at 395 nm. Once the sample was reduced, phenol was tipped into the cuvette from the sidearm to a final concentration of 1.5 mM. For product analysis, an aliquot (0.9 mL) was transferred to a 1.5 mL cuvette and mixed several times to aerate the sample. The yield of catechol was determined by adding 4−5 units of catechol 2,3-oxygenase (the next enzyme in the pathway) and monitoring the formation of α-hydroxymuconic semialdehyde, $\epsilon = 44\,800$ M^{-1} cm^{-1} at 374 nm.

Inactivation of the Oxygenase by Dithiothreitol or Hydrogen Peroxide. Solutions of the oxygenase (1.3−1.4 mg/mL) in 50 mM Tris-HCl, pH 7.5, containing 10% glycerol, were stored at 4 °C in the presence of various additives, and samples were withdrawn periodically for activity assays. The following additions were made: dithiothreitol (1 mM); dithiothreitol (1 mM) and catalase (1000 units); catalase only (1000 units); dithiothreitol (1 mM) and DmpM (9 μM); dithiothreitol (1 mM) and phenol (1.6 mM); DmpM only (9 μM); phenol only (1.6 mM); or hydrogen peroxide (100:1). Prior to assay for activity by coupling with catechol 2,3-dioxygenase, excess H_2O_2 was destroyed by the addition of catalase (1000 units).

Inactivation of reduced oxygenase samples was also examined. Anaerobic samples were prepared as described above for single turnover experiments. Reduction by DTT was examined by titrating DmpLNO (1 mg/mL) in TG buffer with an anaerobic solution of DTT (0.1 M), and monitoring bleaching of the 350 nm band. After the addition of DTT to 6 mM, no bleaching was immediately observed, but after 1 h at 25 °C under anaerobic conditions, reduction appeared to be complete. A portion of the DTT-reduced oxygenase was kept anaerobic, while another was exposed to air, and the two samples were assayed for activity periodically over several days. Anaerobic samples were withdrawn and assayed immediately after exposure to oxygen.

Inactivation of DTT- or dithionite-reduced oxygenase by hydrogen peroxide was tested by adding a 100× molar excess of H_2O_2 to reduced DmpLNO. The DTT-reduced oxygenase treated with H_2O_2 was exposed to air, and the activity was monitored at various times over several days. The dithionite-reduced oxygenase treated with H_2O_2 was kept anaerobic and was also monitored for activity periodically.

Dialysis of the DTT-Inactivated DmpLNO Sample and Reconstitution with Fe^{2+}. The oxygenase reduced with DTT (6 mM) and inactivated by exposure to air for 24 h (described

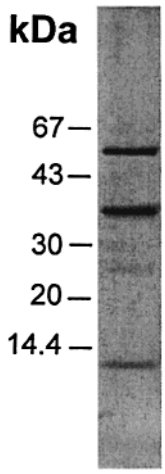

FIGURE 1: SDS−polyacrylamide electrophoresis of the oxygenase component of phenol hydroxylase (10 μg).

above) was dialyzed against 1 L of TG buffer at 4 °C for 2 h. The buffer was changed to fresh TG buffer, and dialysis was continued overnight, after which the sample was assayed for activity. Reconstitution of activity was attempted by adding stoichiometric amounts of Fe^{2+} as ferrous ammonium sulfate to the dialyzed oxygenase sample (1 mg/mL). Activity was monitored over a period of 30 min.

Chemical Cross-Linking with EDC and Sulfo-NHS. Chemical modification of DmpM (2.4 nmol) was carried out in 50 mM MOPS, pH 7.0, with EDC (50 mM) and sulfo-NHS (50 mM) in a total volume of 50 μL. After incubation for 15 min at room temperature, the reaction was stopped by adding β-mercaptoethanol to a final concentration of 50 mM. Oxygenase component in TG buffer (2.4 nmol) was then added and allowed to react for 1 h at room temperature. Control experiments were done by incubating DmpM and the oxygenase component separately with EDC and sulfo-NHS as described above. After the addition of β-mercaptoethanol, equal amounts of the same protein were added to the cross-linking mixture. Reaction products were analyzed by SDS−polyacrylamide gel electrophoresis.

RESULTS

Purification of the Oxygenase Component of Phenol Hydroxylase. Phenol hydroxylase activity has previously been shown to depend on the gene products of dmpKLMNOP (*19*). Purifications of the reductase (DmpP), activator (DmpM), and DmpK components have been reported (*10*−*12*). The oxygenase component was purified as described under Experimental Procedures. Denaturing gel electrophoresis (Figure 1) shows that the protein contains three polypeptides with molecular masses of 39, 60, and 13 kDa, corresponding to DmpL, -N, and -O, respectively (*19*). An unidentified contaminant migrating at 25 kDa consistently appeared in all preparations. While the subunit composition is DmpLNO ($\alpha\beta\gamma$), gel filtration experiments are consistent with the existence of a DmpLNO dimer; however, sedimentation velocity experiments indicate some heterogeneity in oligomeric structure, of which the source is presently under investigation (data not shown).

Activity and Iron Measurements. When purified as described above and assayed under standard conditions (Experimental Procedures), the specific activity of the purified

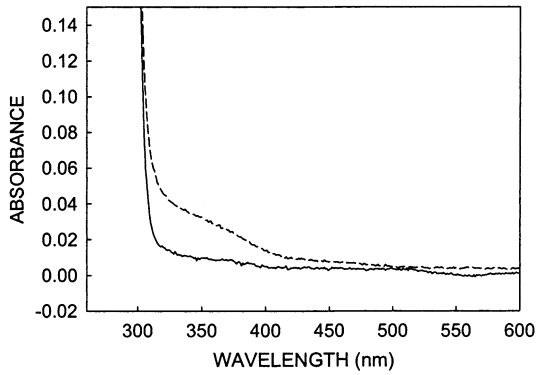

FIGURE 2: Optical spectra of apo- and holo-oxygenase. Apo-oxygenase (—, 1 μg/mL protein, 9 μM protomer); holo-oxygenase (- - -, 1 mg/mL protein, 9 μM protomer). Samples were in 0.05 M Tris-HCl, pH 7.4, containing 10% glycerol.

Table 1: Properties of Purified DmpLNO

prep	[protein] (mM)	[Fe] (mM)	Fe/-$\alpha\beta\gamma$	ϵ_{350nm} (M^{-1} cm^{-1})[a]	act./ binuclear center (min^{-1})	act. (mU/mg of DmpLNO)
49	1.1	1.9	1.8 (85[b])	4800 (5650)[c]	145	1100
48	0.35	0.63	1.8 (87[b])	6000 (6900)[c]	150	1200
44	2.4	3.3	1.4 (77[b])	4800 (6200)[c]	220	1300
43	0.48	0.91	1.7 (85[b])	ND[d]	220	970

[a] Per mole of binuclear iron cluster. [b] Percent of total Fe in cluster I. [c] Extinction coefficient if all absorption is assigned to cluster I. [d] ND: not determined.

oxygenase was found to range between 780 and 1400 nmol min^{-1} mg^{-1}, and the iron content to vary between 1.2 and 1.8 Fe per $\alpha\beta\gamma$. Initially, we purified the oxygenase with dithiothreitol present in the purification buffer, primarily because low molecular weight thiols are routinely used for purification of related proteins. For oxygenase purified in the presence of DTT, the specific activity was consistently lower, ranging from 557 to 923 nmol min^{-1} mg^{-1}, and the iron content ranged between 1.8 and 2.4 Fe/$\alpha\beta\gamma$. Thus, on average, omission of DTT from the purification buffer resulted in higher specific activity but less iron. The nature of inactivation by DTT is examined further below.

UV/Vis Spectra of the Oxygenase Component. Figure 2 shows the optical spectra of the as-isolated oxygenase component and of the apo-oxygenase (protein lacking detectable iron). As will be reported elsewhere, the apo-oxygenase is inactive, which demonstrates the requirement for iron in active enzyme (E. Cadieux and J. Powlowski, manuscript in preparation). Comparison of the spectra of holo- and apo-oxygenases indicates the presence of a shoulder between 320 and 400 nm associated with the presence of iron in the protein. The extinction coefficient at 350 nm was in the interval 4800−6000 M^{-1} cm^{-1} per binuclear iron center (Table 1).

Dependence of Steady-State Turnover Rate on DmpM Concentration. The steady-state rate of phenol hydroxylase turnover is dependent on the DmpM concentration, with a maximum observed rate at about 1.5 DmpM per oxygenase monomer: higher concentrations of DmpM inhibit phenol

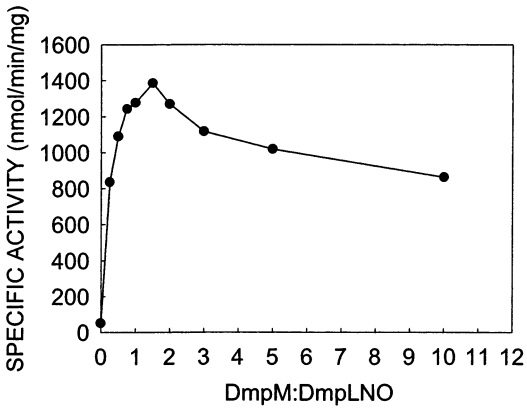

FIGURE 3: Effect of the ratio of DmpM to oxygenase (DmpLNO) on the steady-state turnover of phenol hydroxylase. The steady-state turnover rate of phenol hydroxylase was determined as described under Experimental Procedures, varying the ratio of DmpM to oxygenase component.

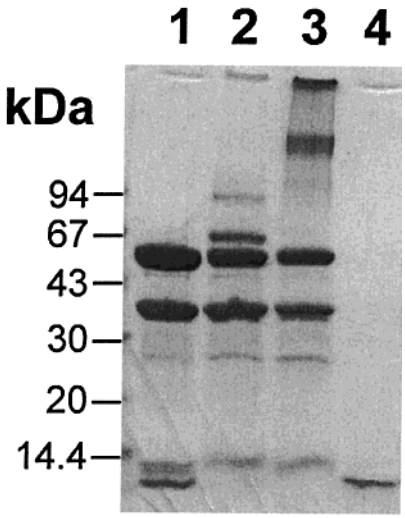

FIGURE 4: SDS−polyacrylamide electrophoresis of the cross-linking reactions of DmpM with the oxygenase component. Lane 1, DmpM (2 μg) and oxygenase component (20 μg) without EDC; lane 2, DmpM (2 μg) and the oxygenase component (20 μg) incubated with EDC; lane 3, oxygenase component (20 μg) incubated with EDC; lane 4, DmpM (2 μg) incubated with EDC.

hydroxylase activity (Figure 3). This behavior is similar to that observed for methane monooxygenase, where MMOB was shown to inhibit at concentrations higher than 2 MMOB per oxygenase monomer (*20*).

Interaction of DmpM with the Oxygenase Revealed by Chemical Cross-Linking. Chemical cross-linking studies of the methane monoxygenase system have shown that the activator protein, MMOB, interacts with the largest subunit of the oxygenase component (*20*). Figure 4 shows the results of cross-linking experiments with the oxygenase and the activator (DmpM) components of phenol hydroxylase. Incubation of oxygenase and DmpM with EDC and sulfo-NHS as described under Experimental Procedures yielded products with molecular masses of 68 and 97 kDa (lane 2) that were not observed in reaction mixtures containing DmpM (lane 4) or oxygenase (lane 3) alone. These cross-linked products are consistent with DmpM (10.3 kDa) complexed with DmpN (58 kDa) and DmpLN, respectively. DmpM in the presence of EDC alone did not yield any cross-linked products, while the oxygenase component treated with

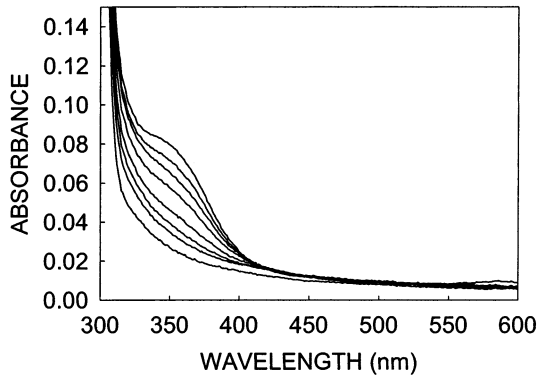

FIGURE 5: Reduction of the oxygenase component by sodium dithionite titration. 8.9 μM protomer of oxygenase component and methyl viologen (1 μM) in 50 mM Tris-HCl, pH 7.45, in a total volume of 2 mL. The oxygenase was titrated with sodium dithionite solution (~2.9 mM) which was prepared in 50 mM HEPES, pH 8.0. The top trace represents the oxidized enzyme.

EDC yielded high molecular weight bands possibly corresponding to a dimer complex of the DmpLNO polypeptides (lane 3).

Single Turnover Experiments. Anaerobic titration of the oxygenase component with sodium dithionite bleached the 350 nm shoulder in the visible spectrum (Figure 5). Readmission of oxygen after adding phenol resulted in the formation of the product, catechol. Efficient product formation required the presence of DmpM, but not the presence of reductase (DmpP). Product yields in the absence and presence of DmpM were 2.3 ± 1.3% and 34 ± 10% per binuclear iron center, respectively; data are the averages of four different oxygenase preparations. Product yields were essentially identical with either 1.5:1 or 5:1 ratios of DmpM to oxygenase active site. These results indicate that the oxygenase is the site of product formation, although productive turnover is inefficient in the absence of the activator protein.

Anaerobic reduction of the oxygenase by NADH and a catalytic amount of DmpP was also attempted. Significant bleaching of the visible spectrum of the oxygenase was observed only in the presence of DmpM (data not shown). This suggests that DmpM alters the redox potential of the oxygenase, as has been reported for methane monooxygenase (*21*).

Mössbauer Studies of the Iron Center. During the last 5 years, we have studied nine preparations of the oxygenase component of phenol hydroxylase with Mössbauer spectroscopy. All samples exhibited two distinct spectral components with proportions that varied somewhat (10%) between preparations. Figure 6 shows 4.2 K spectra obtained from preparation 43 (Table 1). The spectrum of Figure 6A exhibits two quadrupole doublets. The majority species, accounting for 85% of the Fe in the sample, has quadrupole splitting, $\Delta E_Q = 1.73(3)$ mm/s, and isomer shift, $\delta = 0.54(2)$ mm/s; we will refer to this spectral component as cluster form I. The remainder of the iron belongs to a doublet with $\Delta E_Q = 0.79(3)$ mm/s and $\delta = 0.48(2)$, representing cluster form II. After addition of dithionite, the spectrum shown in Figure 6B was observed. Its Mössbauer parameters, $\Delta E_Q = 2.8(1)$ mm/s and $\delta = 1.28(3)$ mm/s, are typical of octahedral high-spin ferrous sites with predominant O-coordination (carboxylate, water). The Mössbauer parameters and the per-

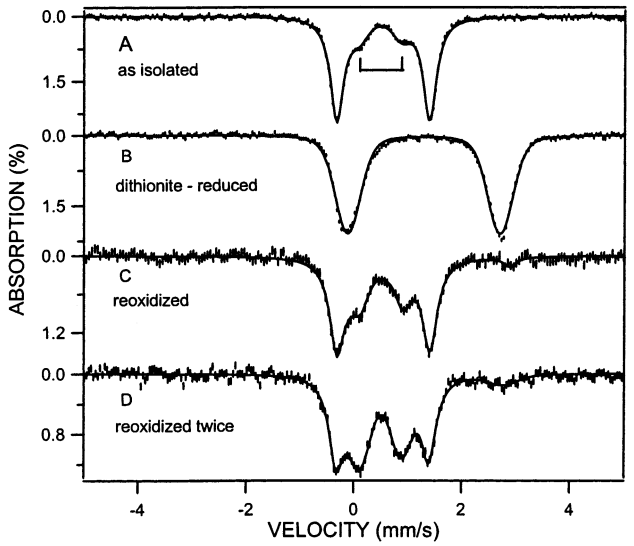

FIGURE 6: Mössbauer spectra of *Pseudomonas* sp. strain CF600 phenol hydroxylase recorded at 4.2 K in the absence of an applied magnetic field. (A) Hydroxylase as isolated; the solid line through the data is a spectral simulation for two doublets with an intensity ratio 85:15; the minority doublet belonging to cluster form II is indicated by the bracket. (B) Sample of (A) after addition of dithionite. The solid line is a spectral simulation assuming one doublet with Voigt line shape. (C) Sample of (B) after reoxidation in air. (D) Sample of (C) after an additional reduction/reoxidation cycle. Solid lines in (C) and (D) are simulations to two doublets with the proportions listed in Table 3. The spectrum of the reduced sample contains unresolved contributions from the four iron sites of cluster forms I and II. We have described these unresolved contributions by using a Voigt shape with 0.55 mm/s Gaussian width.

Table 2: Characterization of Mössbauer Samples of Figures 6 and 12

	diferric			diferrous		
sample	ΔE_Q[a]	δ[a]	%[b]	ΔE_Q[a]	δ[a]	%[b]
as-isolated	1.73(3)	0.54(2)	85(3)			
	0.79(3)	0.48(2)	15(3)			
dithionite-reduced				2.80	1.28	100
one red./reox cycle	1.73	0.54	62(4)	≈3.1	1.3	5
	0.79	0.48	33(4)			
two red./reox cycles	1.73	0.54	41(4)	2.8	1.3	8
	0.79	0.48	51(4)			
as-isolated+DTT	1.92	0.39	46	2.8−2.9	≈1.3	8[c]
	0.53	0.34	46			

[a] In mm/s. Isomer shifts are quoted relative to Fe metal at 298 K. [b] Percent of total Fe in sample. [c] High-spin Fe^{2+}, not necessarily diferrous.

centage of iron belonging to each cluster form are listed in Table 2.

The presence of quadrupole doublets in the spectrum of Figure 6A, coupled with the observation of high-spin ferrous sites generated by reduction with dithionite, indicates spin-coupled high-spin ferric sites similar to those observed in diiron proteins. The 8.0 T spectra shown in Figure 7A confirm this assignment. These spectra were obtained from a preparation for which the zero-field spectrum indicated a 70:30 ratio for the doublets of clusters I and II. The solid line drawn through the spectrum of Figure 7A is a theoretical curve generated by assuming that the iron of both cluster forms resides in diamagnetic sites; the good match of the

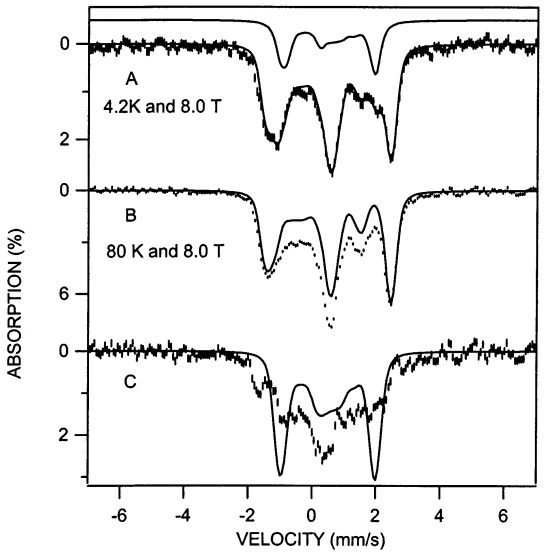

FIGURE 7: Mössbauer spectra of an oxidized sample of phenol hydroxylase recorded in 8.0 T fields applied parallel to the observed γ-rays. For this sample 70% of the Fe(III)Fe(III) clusters were found to belong to form I and 30% to form II. The solid line in (A) is a spectral simulation assuming that the iron sites in each cluster form are equivalent and that the electronic ground state of both cluster forms is diamagnetic. For cluster form I, we used $\Delta E_Q = -1.75$ mm/s and $\eta = 0.35$ for the asymmetry parameter, and for cluster form II, $\Delta E_Q = 0.80$ mm/s and $\eta = 0.40$. The simulation for cluster II is shown separately, above the data. The spectrum in (B) was recorded at 80 K. The solid line is a simulation of the spectrum for cluster form I (70% of Fe) assuming that only the $S = 0$ ground state is populated. The spectrum shown in (C) was obtained by subtracting the simulated spectrum of cluster I from the experimental spectrum of (B). The solid line in (C) is a simulation [same curve as shown above (A)], demonstrating that the 80 K spectrum of form II has contributions from excited states of the spin ladder (essentially $S = 1$ and $S = 2$ states).

theoretical curve with the experimental splittings confirms this assumption. The chemical nature of the ligands bridging the two iron sites can be assessed by estimating the exchange coupling constant J ($H = J\mathbf{S}_1\cdot\mathbf{S}_2$). The spectrum shown in Figure 7B was recorded at $T = 80$ K in an 8.0 T parallel field. Close inspection of the data reveals that the spectrum of cluster I is the same at 4.2 and 80 K, showing that excited states of the spin ladder are not measurably populated at 80 K. From analysis of the 80 K spectrum using a spin coupling model (the method has been described elsewhere; see text and Figure 8 of ref *22*), we conclude that $J > 120$ cm^{-1} for cluster I. In contrast, the spectra of cluster II change considerably between 4.2 and 80 K. This is illustrated in Figure 7C, which shows the 80 K spectrum of cluster II obtained by subtracting the simulation of form I from the experimental spectrum.

The shape of the 80 K spectrum of cluster II is actually quite similar to intermediate-relaxation spectra we have observed for the hydroxylase component of methane monooxygenase (MMOH). The observation of temperature-dependent, high-field spectra for cluster II indicates that low-lying states of the spin ladder are appreciably populated at 80 K (broadening is already seen at 30 K), implying that cluster II has a substantially smaller J than form I. The general features of the spectrum of Figure 7C suggest intermediate fluctuation rates of the electronic spin; under these conditions, the spectra are exceedingly difficult to analyze for the present case.

Table 3: Activity for Mössbauer Sample, Initially and after Redox-Cycling

	% activity	% cluster I
sample 1	100	85
reoxidation 1	77	62
reoxidation 2	61	41

To summarize, the spectra of the oxidized hydroxylase exhibit two spectral components. These components cannot originate from one cluster. First, their proportions vary between different preparations, and, moreover, the spectral components are associated with sites that are constituents of spin-coupled Fe(III)Fe(III) clusters with substantially different *J*-values. Each cluster form contributes, in the absence of an applied field, *one* quadrupole doublet, indicating that the two irons in each cluster form have very similar ligand structure. This is particularly true for cluster I which exhibits a sharp doublet with 0.30 mm/s line width (full width at half-maximum); our analysis indicates that the ΔE_Q-values of the two sites of the cluster can differ by at most 5%, if they differ at all. Thus, the cluster binding sites of the hydroxylase dimer can accommodate two distinct binuclear clusters. Our data suggest that the two cluster forms have different bridging ligands for the two cluster forms because the two iron sites in each cluster form are equivalent and because the sites in the two forms differ substantially. The large *J*-value observed for cluster form I is consistent with a μ-oxo-bridged structure whereas the smaller *J*-value of cluster form II is reminiscent of the hydroxo-bridged MMOH cluster.

To test whether both cluster forms are catalytically active, we have carried the sample of Figure 6 through two reduction/reoxidation cycles (see Experimental Procedures). The spectra of Figure 6C,D were recorded after one and two reduction/reoxidation cycles, respectively. It can be seen that a fraction of form I has been converted to form II after each cycle; after two cycles, the proportion of Fe in cluster form I has decreased from 85% to 40%. As shown in Table 3, the catalytic activity as measured in the standard assay correlates quite well with the amount of cluster I present in the oxidized form of the enzyme.

EPR of Reduced Phenol Hydroxylase. The electronic spins of diferrous clusters ($S_1 = S_2 = 2$) are generally coupled by weak exchange interactions, $H = J\mathbf{S}_1\cdot\mathbf{S}_2$, to produce a system comprising 25 closely spaced spin levels; "weak" refers to the case where the magnitude of *J* is smaller than the zero-field splitting parameters, *D*, of the ferrous ions. If a pair of spin levels is separated by an energy Δ smaller than $h\nu = 0.30\ \text{cm}^{-1}$, one may observe at X-band an integer spin EPR transition. For reduced methane monooxygenase from *M. trichosporium*, the integer spin EPR spectra have been analyzed in considerable detail (*23*), and Lipscomb and coworkers have used EPR to study the reaction of reduced MMOH with substrate and the effector protein component B (*20*, *24*). A similar integer spin signal has also been reported for the oxygenase component of toluene-4-monooxygenase (*25*).

To examine whether reduced phenol hydroxylase exhibits an EPR signal, we have reduced an ^{57}Fe-enriched sample that contained 85% of the iron in cluster I and 15% in cluster II and studied it at 4.2 K with Mössbauer spectroscopy in

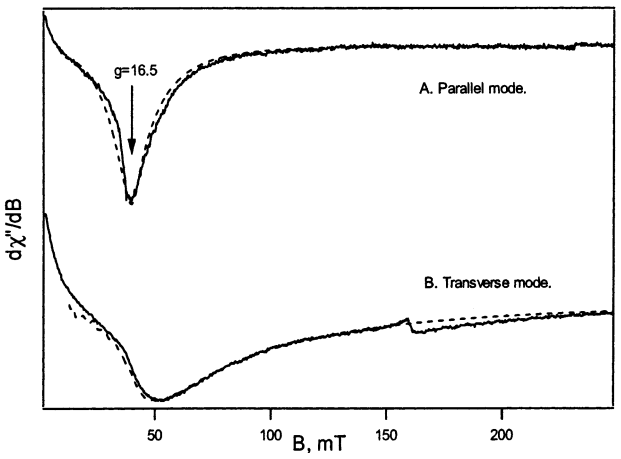

FIGURE 8: EPR spectra of dithionite-reduced phenol hydroxylase recorded at 2.1 K with the microwave field B_1 applied parallel (A) and perpendicular (B) to the static magnetic field. Diiron cluster concentration, 0.73 mM. (Prior to reduction, 85% of the clusters were in form I and 15% in form II.) Experimental conditions: microwave frequency, 9.26 GHz in parallel mode and 9.62 GHz in perpendicular mode; microwave power, 20 μW; modulation, 100 kHz at 0.98 mT (pp). The solid lines are spectral simulations using the $S = 4$ spin Hamiltonian of eq 1 for $D = 1.05\ \text{cm}^{-1}$, $E/D = 0.10$ (corresponding to $\Delta_0 = 0.36\ \text{cm}^{-1}$), $\sigma_{E/D} = 0.045$, $g_x = g_y = g_z = 2.00$. All amplitude factors, except the spin concentration (0.14 mM), were determined by calibrating the detection system with known spin standards.

applied fields up to 8.0 T. The spectra obtained (not shown) were quite complex and poorly resolved. We have not yet analyzed these data (more than 40 unknown parameters have to be determined). However, spectra recorded at 0.6 and 1.0 T revealed that one of the clusters, most likely cluster II, exhibits considerable hyperfine splittings in these relatively weak applied fields. This observation indicates that one of the clusters has an electronic system such that the two lowest spin levels are separated in energy by $\Delta \approx 0.3\ \text{cm}^{-1}$, suggesting that one might observe an integer spin EPR signal at X-band. Figure 8 shows $T = 2.1$ K EPR spectra of the sample studied with Mössbauer spectroscopy recorded with the microwave field B_1 applied either parallel (A) or perpendicular (B) to the static field *B*. At 2.1 K, the signals saturate readily at microwave powers larger than 20 μW, in particular for $B < 20$ mT. The broad features of the signals indicate that the splitting parameter Δ is distributed (the portion of the signal below $B < 20$ mT originates from molecules whose Δ-values approach the energy of the microwave quantum). The intensities of the observed signals decline as the temperature is raised, showing that the EPR-active doublet is the ground state, in agreement with the conclusion reached by considering the response of the Mössbauer spectra to weak applied magnetic fields. At 8 K, the signals can be observed at microwave powers up to 200 μW without saturation. Within the uncertainties (temperature and baseline variations), the EPR intensity follows a $1/T$ dependence between 2.1 and 8 K, suggesting that in this temperature interval only the EPR active doublet is populated.

The shapes of the signals shown in Figure 8 suggest that they represent one spin system; i.e., only one of the two cluster forms contributes to the spectra. To fully describe the EPR spectra of a diferrous cluster, one has to take into account, for each iron site, the electronic **g**-tensor and the

zero-field splitting tensor and perhaps sets of angles that specify the relative orientation of the four tensors (for details, see *23*, *26*). Based on data reported for other diiron proteins, it can be anticipated that spins of the two iron sites are weakly exchange-coupled (*23*, *27*, *28*). The Mössbauer spectra of the reduced enzyme suggest that the coupling is ferromagnetic. If we restrict ourselves to analyzing the 2.2 K spectra, i.e., to conditions where only the two lowest spin levels are measurably populated, quantitative analysis of the spectra can be achieved by considering only the quasi-degenerate doublet with splitting Δ. This situation can be described with an effective Hamiltonian with $S = 1/2$ (*29*). Under these conditions, the EPR spectra depend only on Δ, on one component of the **g**-tensor, and on the distribution of Δ about its mean value Δ_0. Alternatively, we can use a spin Hamiltonian for integer spin *S*, choosing zero-field splitting parameters (*D* and *E*) and one component of the **g**-tensor (g_y in eq 1) such that the Hamiltonian produces a quasi-degenerate ground doublet with the observed EPR properties. In this case, the distribution of Δ corresponds to a distribution in *E/D* and/or *D*. Although the parameters obtained will not describe all aspects of the real system, the description yields the correct EPR transition probabilities between the two spin levels and thus allows determination of the spin concentration, enabling us to decide whether cluster I or cluster II yields the observed EPR signals. For the simulation of the spectra of Figure 8, we have chosen the $S = 4$ Hamiltonian:

$$H = D[\mathbf{S}_z^2 - S(S+1)/3 + E/D(\mathbf{S}_x^2 - \mathbf{S}_y^2)] + \beta \mathbf{S}\cdot\mathbf{g}\cdot\mathbf{B} \quad (1)$$

(This Hamiltonian is realistic if the ferromagnetic exchange coupling constant *J* is comparable to or larger than the zero-field splittings of the ferrous ions.) For $D = 1.05$ cm^{-1}, $E/D = 0.10$, and $g_y = 2.0$, the Hamiltonian of eq 1 produces two low-lying spin levels spaced by $\Delta_0 = 0.36$ cm^{-1} for which a parallel mode resonance at $g = 16.5$ would be observed; the two spin levels are mainly composed of the $\phi^0 = |M_S = 0\rangle$ and $\phi^- = (|M_S = +1\rangle - |M_S = -1\rangle)/\sqrt{2}$ states, but admixtures of states with $|M_S| > 1$ levels matter also. By assuming that the parameter *E/D* has a Gaussian distribution about its mean $E/D = 0.10$ with $\sigma_{E/D} = 0.045$, an excellent simulation of the line shape is obtained both in parallel and in perpendicular modes. A spin concentration of 0.14 mM matches the amplitudes in both parallel and transverse modes. Metal analysis of the sample gave an iron concentration of 1.46 mM. Since the Mössbauer data did not reveal any iron other than that attributable to the two binuclear clusters, the total cluster concentration was 0.73 mM. Thus, the spin concentration determined by EPR accounts for 19% of the cluster concentration. Within the uncertainties, this value corresponds quite well to the 15% attributed to cluster II by Mössbauer spectroscopy. It is noteworthy that for $\Delta_0 = 0.36$ cm^{-1}, less than half of the molecules of cluster II have Δ-values sufficiently small to yield an EPR transition at X-band (see, for instance, ref 26).

Study of the Hamiltonian (eq 1) shows that the EPR spectra should essentially be independent of g_x and g_z, and for the spectral simulations we have therefore set $g_x = g_z = 2.00$. It should be noted that Δ_0 and g_y cannot be determined independently if the samples are studied at only one microwave frequency. [The resonance condition for the quasi-degenerate doublet is $(h\nu)^2 = \Delta^2 + (g_{\text{eff}} \cos \alpha\, \beta B)^2$, where α is the angle between the static field and the molecular *y*-axis and g_{eff} is an effective *g*-value that depends on g_y and *E/D*.] Also, study of the exchange-coupled Hamiltonian involving the spins of the two ferrous ions reveals that for ferromagnetic coupling the lowest energy levels are reasonably well-defined by an $S = 4$ multiplet, provided that $|J|$ is comparable to or larger than the *D*-values of the two ferrous sites.

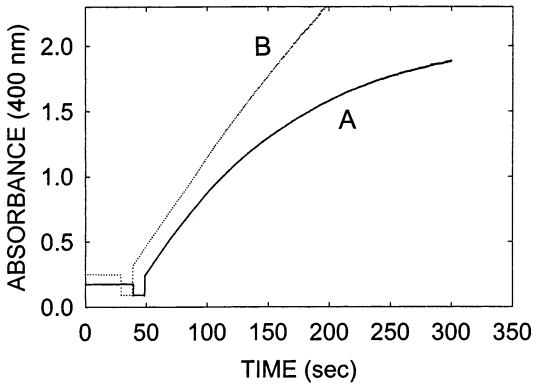

FIGURE 9: Steady-state turnover of phenol hydroxylase with and without added catalase (200 units), monitored by the appearance of 2-hydroxymuconic semialdehyde at 400 nm. Phenol hydroxylase activity in the absence (A) and presence of 200 units of catalase (B). Activity assays were done as described elsewhere (*12*) except that the phenol concentration was 150 μM.

Table 4: Reduction and Reoxidation of the Oxygenase (DmpLNO)

	% activity		
reductant	Reox1	Reox2	Reox3
dithionite	97	82	66
NADH	ND[a]	ND	ND
dithionite + DmpM	95	87	75
NADH + DmpM	83	75	70

[a] ND: Not detectable.

Inactivation of Oxygenase by Turnover and Dithiothreitol. The variability in activity that is observed from preparation to preparation is not completely explained by the relative iron center content of the oxygenase. The Mössbauer studies indicate the presence of variable amounts of two cluster forms, one of which appears to be inactive. However, the origins of the two forms are not known. We undertook to investigate what factors contribute to the inactivation of the oxygenase.

Steady-state turnover of phenol was accompanied by progressive loss of activity (Figure 9). Once product formation slowed, it was not stimulated by the addition of more coupling enzyme, catechol 2,3-dioxygenase, indicating that it is not the coupling enzyme that is being inactivated (data not shown). However, inclusion of catalase markedly improved the linearity of these assays (Figure 9), suggesting that the enzyme is inhibited by the accumulation of hydrogen peroxide. Inactivation was also observed under single turnover conditions in the absence of substrate and DmpM. As the enzyme was cycled between reduced and oxidized forms, activity was progressively lost (Table 4): these results are similar to those shown in Table 3 for redox-cycled Mössbauer samples. Inactivation thus appears to be related

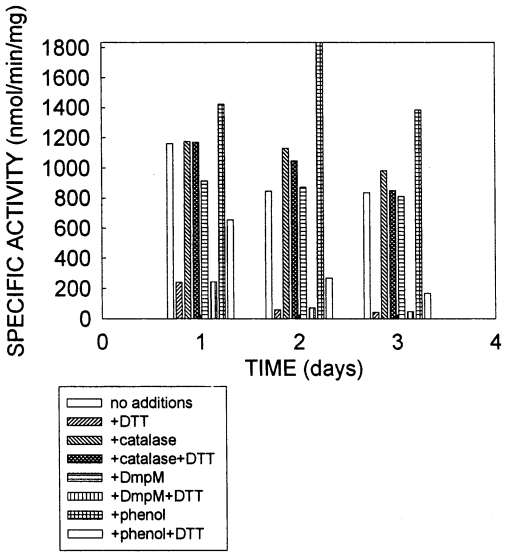

FIGURE 10: Inactivation of the oxygenase component with dithiothreitol. Samples were prepared as described under Experimental Procedures, and aliquots were periodically assayed for phenol hydroxylase activity. The concentrations of additives were: DTT, 1 mM; catalase, 1000 units; phenol, 1.6 mM; and DmpM, 9 μM.

to formation of an activated oxygen intermediate, such as hydrogen peroxide, after turnover in the absence of substrate.

The observation that lower specific activity was associated with the presence of DTT in purification buffers (see above) suggested that DTT could also contribute to the generation of an inactive form of the enzyme. This possibility was examined more closely by incubating purified enzyme with DTT, and monitoring the activity over a period of time.

The presence of DTT caused large losses in the activity of the oxygenase: protection against these losses was afforded by the inclusion of catalase (Figure 10). Addition of DmpM or phenol to the sample containing DTT did not protect the oxygenase from inactivation (Figure 10). Protection by catalase suggests that DTT has its effect by acting as a peroxide generator, as has been previously observed for lipoxygenase (*30*, and references cited therein). In the case of lipoxygenase, the authors postulated that hydrogen peroxide is generated by DTT and that the reaction of the active-site Fe^{2+} with H_2O_2 generates an active oxygen species which could react with a side chain of an amino acid residue at the active site. Interestingly, in the case of phenol hydroxylase, hydrogen peroxide itself did not inhibit the oxygenase when incubated with it under aerobic conditions (Figure 11A). However, incubation of the dithionite-reduced oxygenase with hydrogen peroxide under anaerobic conditions resulted in inactivation (Figure 11A). These data suggest that inactivation by hydrogen peroxide occurs specifically with the reduced form of the enzyme.

It is therefore of interest to know whether the oxygenase diiron center can be reduced by DTT. When DTT was added to the oxygenase component under anaerobic conditions, slow bleaching of the 350 nm band indicated reduction of the binuclear iron center (data not shown). The reduced sample was assayed periodically for activity over several days of storage under anaerobic conditions, and was found to retain it over a 24 h period unless O_2 was admitted (Figure 11B). These data suggest that inactivation of the enzyme with DTT involves reduction of the diiron center followed

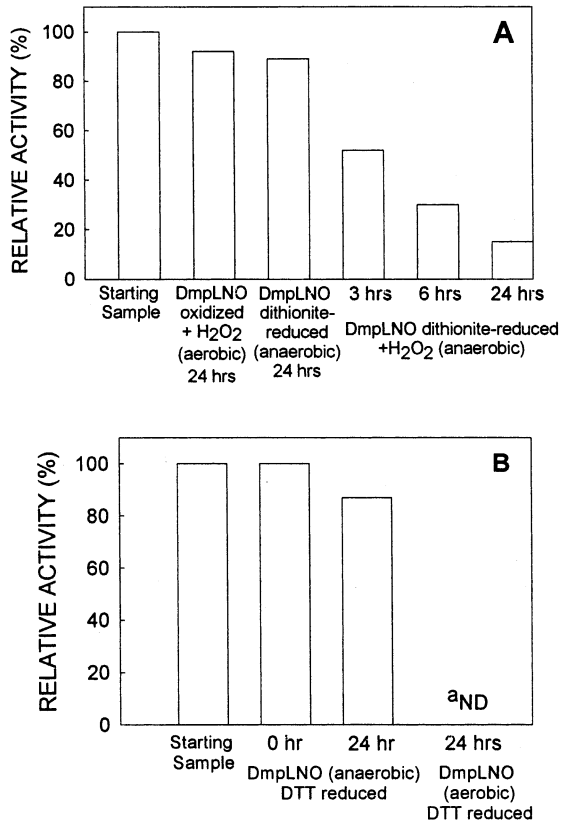

FIGURE 11: Inactivation of DmpLNO by H_2O_2. (A) H_2O_2 (100:1 molar ratio of hydrogen peroxide to DmpLNO monomer) was added to oxidized aerobic DmpLNO (1 mg/mL) or anaerobic DmpLNO reduced with sodium dithionite (as described under Experimental Procedures). Phenol hydroxylase activity was monitored over time with assays done in duplicate. Relative activity is the percentage activity relative to a fresh untreated DmpLNO sample. (B) DmpLNO (1 mg/mL) was reduced with excess dithiothreitol (see Experimental Procedures) and kept anaerobic. After 24 h, the sample was exposed to air, and activity was monitored. [a]ND, not detectable.

by a reaction with some form of oxygen: protection of inactivation by catalase (see above) suggests that hydrogen peroxide may be that form.

To test whether inactivation by DTT is related to loss of the iron from the binuclear iron center, the DTT-inactivated sample described in Figure 11B was dialyzed against TG buffer to remove excess DTT and iron not bound to the protein. Activity was not regained after dialysis, and addition of Fe^{2+} to this sample did not activate the enzyme. These data suggest that the DTT-inactivated sample is not an apo form generated by removal of the binuclear irons by DTT.

Mössbauer Spectroscopy of DTT-Inactivated Oxygenase. The DTT-associated inactivation mechanism was probed further by preparing a Mössbauer sample of oxidized enzyme in the presence of a large excess of DTT (see Experimental Procedures). Figure 12A shows a 4.2 K, zero-field Mössbauer spectrum of this sample. The spectrum exhibits two major doublets and a minority species. Doublet a, representing ca. 45% of total Fe, has $\Delta E_Q(a) = 1.92$ mm/s and $\delta(a) = 0.39$ mm/s, while doublet b, also ca. 45% of Fe, has $\Delta E_Q(b) = 0.53$ mm/s and $\delta(b) = 0.35$ mm/s. The sample also contains a minor (6%) high-spin ferrous species with $\Delta E_Q = 2.9$ mm/s and $\delta = 1.3$ mm/s, reflecting either reduced binuclear centers or adventitiously bound Fe. The isomer shifts of species a and b are substantially less than those of the native diferric

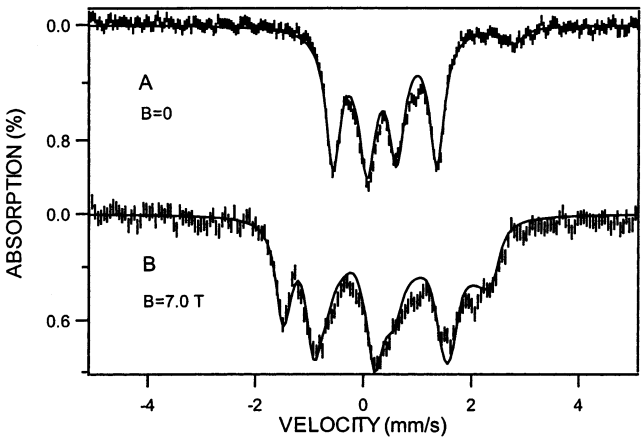

FIGURE 12: Mössbauer spectra of diferric phenol hydroxylase incubated with excess DTT. The spectra were recorded at 4.2 K in zero field (A) and a parallel field of 7.0 T (B). The solid lines are simulations using the parameters quoted in Table 3, and for η the values $\eta(a) = \eta(b) = 0$.

centers, suggesting thiolate coordination. Moreover, the observation of equal intensities for doublets a and b suggests that the two species are still constituents of a diferric center. That this is indeed the case is attested by the 7.0 T spectrum of Figure 12B, which shows that species a and b are diamagnetic. As monomeric ferric iron is paramagnetic, the iron represented by species a and b must belong to an antiferromagnetically coupled binuclear center. Since the two Fe sites have low isomer shifts, both are probably coordinated to at least one thiolate. After completion of the Mössbauer study of the DTT-treated sample, the protein was dialyzed twice against TG buffer to remove excess DTT and iron not bound to the protein. The Mössbauer spectrum observed after dialysis was the same as that shown in Figure 12A, showing that the cluster observed in the spectra of Figure 12 is protein-bound. Moreover, the data show that cluster-bound DTT is not removed by dialysis.

DISCUSSION

The present work has shown that the oxygenase component of phenol hydroxylase from *Pseudomonas* sp. strain CF600 is a dimeric protein composed of three subunits, DmpL, DmpN, and DmpO, and containing a diiron center active site. Phenol hydroxylase is thus similar to other diiron-cluster-containing monooxygenases such as methane monooxygenase from *Methylococcus capsulatus* (Bath) or *Methylosinus trichosporium* OB3b (*5*), toluene-2-monooxygenase from *Burkholderia cepacia* G4 (*31*), and toluene-4-monooxygenase from *Pseudomonas mendocina* KR1 (*25*). The DmpN polypeptide contains the amino acid sequence motif assigned to the ligands of a diiron center. This motif was originally assigned in conjunction with various spectroscopic and X-ray crystallography data of the hydroxylase component of methane monooxygenase (*32*, *33*). We have now confirmed the presence of a diiron cluster by using Mössbauer spectroscopy.

Methane and toluene monooxygenases lack an optical spectroscopic feature between 300 and 800 nm, and published data suggest the presence of a hydroxo-bridged diiron cluster in these proteins (*5*, *25*). In contrast, the oxygenase component of phenol hydroxylase exhibits a broad shoulder between 320 and 400 nm. This feature is reminiscent of the characteristic ligand to metal charge-transfer interactions of the oxo-bridged diiron centers present in ribonucleotide reductase (*34*) and stearoyl-ACP Δ^9-desaturase (*35*, *36*). This optical feature along with the Mössbauer data suggest that the diiron cluster of phenol hydroxylase contains an oxo bridge. The mechanistic significance of the bridge variation in different oxygenases has not yet been defined.

DmpM shares amino acid sequence similarity with the well-characterized component B (MMOB) of the *M. capsulatus* and *M. trichosporium* OB3b methane monooxygenases (*37*). MMOB has been shown to have multiple effects on methane monooxygenase including: increasing rate and yield in steady-state turnover (*20*, *38*); perturbation of the EPR properties of the diiron center (*20*, *24*); changing the redox potential of the diiron center (*21*, *39*, *40*); affecting the product distribution with isopentane as a substrate (*24*); and increasing the rate of association of the diferrous hydroxylase with O_2 (*41*). MMOB was shown to form a cross-linked product with the binuclear iron center bearing subunit of the hydroxylase component of methane monooxygenase from *M. trichosporium* OB3b (*20*). Similarly, chemical cross-linking with EDC showed that DmpM interacts with the diiron center containing polypeptide, DmpN, of the oxygenase component. DmpM also had significant effects on both the steady-state turnover rate and the product yield during single turnover reactions.

The single turnover experiments reported here confirm that the site of phenol hydroxylation is on the oxygenase component of phenol hydroxylase, although product yields are very low in the absence of DmpM. Addition of DmpM dramatically increased the product yield, although it never exceeded 40% for any given preparation. Low yields during single turnover reactions have also been reported for toluene-4-monooxygenase from *Pseudomonas mendocina* KR1, where 8% product formation in the presence of activator protein was reported (*25*). Also, methane monoxgygenase from *M. trichosporium* yielded 40% product after single turnover in the absence of MMOB, increasing to 80% upon addition of MMOB (*41*). Low yields may result from the presence of inactive hydroxylase and/or uncoupling reactions during turnover of the enzyme. In this work, we have shown that all phenol hydroxylase preparations contain a proportion of apparently inactive species (molecules bearing cluster II), which could contribute to the low yields observed after single turnover.

The Mössbauer studies show that phenol hydroxylase can accommodate two kinds of binuclear clusters. The two iron sites in each Fe(III)Fe(III) cluster are indistinguishable by Mössbauer spectroscopy, but the ΔE_Q-values for clusters I ($\Delta E_Q = 1.73$ mm/s) and II ($\Delta E_Q = 0.79$ mm/s) differ substantially. ΔE_Q-values larger than 1.5 mm/s have been found for μ-oxo-bridged clusters such as those found in *E. coli* ribonucleotide reductase (*42*), *Ricinus communis* Δ^9-desaturase (*36*), and rubrerythrin (*43*), whereas ΔE_Q-values between 0.7 and 1.1 mm/s seem to be associated with hydroxo/water-bridged clusters such as those observed in MMOH (see *5*) and toluene-4-monooxygenase (*25*). Against this background cluster forms I and II represent μ-oxo- and hydroxo (or water)-bridged clusters, respectively. This assignment is also supported by the estimated exchange coupling constants. *J*-values of oxo-bridged Fe(III)Fe(III) complexes fall into the $150-250$ cm^{-1} range (*44*), and by

combining our lower limit of J (120 cm^{-1}) with $\Delta E_Q = 1.75$ mm/s, we conclude that the iron sites of the ferric hydroxylase are bridged by a μ-oxo group (perhaps supported by one or two bridging carboxylates). This assignment is supported by the UV/visible spectra, which exhibit a broad feature centered around 350 nm. For three samples studied extensively with Mössbauer spectroscopy, the extinction coefficient at 350 nm varied between $\epsilon = 4800$ and 6000 M^{-1} cm^{-1} (or between 5450 and 6900 M^{-1} cm^{-1} if ϵ is solely attributed to the contribution of cluster I). These values compare quite well with ϵ(350 nm) $\approx$ 5000 M^{-1} cm^{-1} reported for $[Fe(III)_2O(OAc)_2(Me_3Tacn)_2]^2$ and ϵ(325−375 nm) $\approx$ 8000 M^{-1} cm^{-1} observed for oxidized ribonucleotide reductase (*34*). Based on magnetic circular dichroism and resonance Raman studies, the latter transitions have been assigned to oxo-to-Fe charge-transfer transitions (*45*).

The observation of two cluster forms in diiron proteins is not unprecedented. In fact, the two cluster forms observed here are very similar to those observed in Δ^9-desaturase for which a sample characterized by Mössbauer spectroscopy and EXAFS exhibited two doublets with $\Delta E_Q = 1.53$ mm/s (μ-oxo form, 72%), $\Delta E_Q = 0.72$ mm/s (μ-hydroxo form, 21%) and a minor form ($\approx$7%) with $\Delta E_Q = 2.20$ mm/s (*36*, *46*). For the desaturase, the proportions of the two major forms were independent of pH between 6 and 10, showing that the cluster is sheltered from the solution and its state is not sensitive to the pH of the solution. Two species have also been observed for toluene-4-monooxygenase, with the hydroxo-bridged form ($\Delta E_Q = 0.93$ mm/s, 85%) being the majority species; the minority species (15%) had $\Delta E_Q = 1.55$ mm/s (*25*). Liu et al. have reported that MMOH isolated from *Methylococcus capsulatus* (Bath) contains two major forms of which only one (32% of Fe) was apparently active as assessed by kinetic studies (*47*).

It is well documented from crystallographic studies of methane monooxygenase that exogenous molecules such as acetate, methanol, ethanol, and dimethyl sulfoxide can serve as bridging ligands of the binuclear center (reviewed in *5*). It is generally not obvious whether a certain cluster form observed in the diferric state will be active because the cluster has to be reduced into the diferrous form before it reacts with oxygen and substrate. The X-ray structure of the Δ^9-desaturase shows a bis(carboxylato)-bridged cluster in the reduced form. Thus, one might be tempted to conclude that it does not matter whether there is an oxo or a hydroxo bridge in the diferric state. However, the diferrous form studied with crystallography resulted through photoreduction by the X-ray beam of the diferric state, and may thus not represent the diferrous state present in solution (*46*). It can also be said the presence of a (hydrogen-bonded) hydroxo bridge could impose a protein conformation that might persist a considerable time. That hydroxylases can sustain altered conformations for a substantial amount of time has been shown by Lipscomb and co-workers (*24*).

In the present study, we have found that the activity, as measured in the assay described under Experimental Procedures, is proportional to the concentration of the oxo-bridged cluster form. The observation that the activity, measured at room temperature, of a given preparation correlates well with the amount of cluster form I observed by Mössbauer spectroscopy at 4.2 K rules out the possibility that cluster form II is a freezing artifact. As pointed out above, we do not know in which step of the reduction/oxidation cycle the conversion to cluster form II occurs. We may speculate that the conversion occurs during reoxidation and it involves a step in the mechanism that differs substantially from the catalytic cycle followed in the presence of DmpM and substrate. It will be important to discover how the cluster transformation can be reversed. Given that the active form of MMOH contains a hydroxo-bridged cluster in the oxidized state, we were initially surprised to learn that the catalytic activity of phenol hydroxylase is proportional to the amount of cluster form I. However, since little is known about the extent to which a hydroxo bridge, observed in the diferric state of the cluster, affects the reaction steps that commence upon reduction and DmpM and substrate binding, we are not in a position to comment on this point.

By studying the oxygenase in the oxidized state with Mössbauer spectroscopy, and by using integer spin EPR coupled with determination of the spin concentration to investigate the reduced samples, it is now possible to keep track of the fractions of clusters I and II in both oxidation states. The Mössbauer spectra of the *reduced* enzyme are not sufficiently resolved to distinguish between clusters I and II. Finally, the isomer shift of the iron sites of the cluster in the protein incubated with excess DTT indicates that DTT binds to the diiron cluster, most likely as a bridging ligand. Another possibility, perhaps less likely, is that DTT molecules coordinate to each iron site in a nonbridging fashion.

ACKNOWLEDGMENT

We thank Donald Tito for technical assistance and Dr. Brian Fox for helpful discussions.

REFERENCES

1. Dagley, S. (1986) in *The Bacteria* (Sokatch, J. R., and Ornston, L. N., Eds.) pp 527−555, Academic Press, London.
2. Palfey, B., Ballou, D. P., and Massey, V. (1995) in *Reactive Oxygen Species in Biochemistry*, Vol. II, pp 37−83, Chapman and Hall, New York.
3. Lange, S. J., and Que, L., Jr. (1998) *Curr. Opin. Chem. Biol. 2*, 159−172.
4. Coulter, E. D., and Ballou, D. P. (1999) *Essays Biochem. 34*, 31−49.
5. Merkx, M., Kopp, D. A., Sazinsky, M. H., Blazyk, J. L., Müller, J., and Lippard, S. J. (2001) *Angew. Chem., Int. Ed. Engl. 40*, 2782−2807.
6. Gallagher, S. C., Cammack, B., and Dalton, H. (1997) *Eur. J. Biochem. 247*, 635−641.
7. Small, F. J., and Ensign, S. A. (1997) *J. Biol. Chem. 272*, 24913−24930.
8. Powlowski, J., and Shingler, V. (1994) *Biodegradation 5*, 219−236.
9. Teramoto, M., Futamata, H., Harayama, S., and Watanabe, K. (1999) *Mol. Gen. Genet. 262*, 552−558.
10. Powlowski, J., and Shingler, V. (1990) *J. Bacteriol. 172*, 6834−6840.
11. Cadieux, E., and Powlowski, J. (1999) *Biochemistry 38*, 10714−10722.
12. Powlowski, J., Sealy, J., Shingler, V., and Cadieux, E. (1997) *J. Biol. Chem. 272*, 945−951.
13. Philo, J. S. (2000) *Anal. Biochem. 179*, 151−163.
14. Brown, R. E., Jarvis, K. L., and Hayland, K. J. (1989) *Anal. Biochem. 180*, 136−138.
15. Gill, S. C., and von Hippel, P. H. (1989) *Anal. Biochem. 182*, 319−326.
16. Percival, M. D. (1991) *J. Biol. Chem. 266*, 10058−10061.
17. Laemmli, U. K. (1970) *Nature (London) 227*, 680−685.
18. Schagger, H., and von Jagow, G. (1987) *Anal. Biochem. 166*, 368−379.

19. Nordlund, I., Powlowski, J., and Shingler, V. (1990) *J. Bacteriol. 172*, 6826−6833.
20. Fox, B., Liu, Y., Dege, J. E., and Lipscomb, J. D. (1991) *J. Biol. Chem. 266*, 540−550.
21. Paulsen, K. E., Lui, Y., Fox, B. G., Lipscomb, J. D., Münck, E., and Stankovich, M. T. (1994) *Biochemistry 33*, 713−722.
22. Kauffmann, K. E., Popescu, C. V., Dong, Y., Lipscomb, J. D., Que, L., Jr., and Münck, E. (1998) *J. Am. Chem. Soc. 120*, 8739−8746.
23. Hendrich, M. P., Münck, E., Fox, B. G., and Lipscomb, J. D. (1990) *J. Am. Chem. Soc. 112*, 5861−5865.
24. Froland, W. A., Andersson, K. K., Lee, S. K., Liu, Y., and Lipscomb, J. D. (1992) *J. Biol. Chem. 267*, 17588−17597.
25. Pikus, J. D., Studts, J. M., Achim, C., Kauffmann, K. E., Münck, E., Steffan, R. J., McClay, K., and Fox, B. G. (1996) *Biochemistry 35*, 9106−9119.
26. Münck, E., Surerus, K. K., and Hendrich, M. P. (1993) *Methods Enzymol. 227*, 463−479.
27. Yang, Y.-S., Baldwin, J., Ley, B. A., Bollinger, M., and Solomon, E. I. J. (2000) *J. Am. Chem. Soc. 122*, 8495−8510.
28. Juarez-Garcia, C. (1990) Ph.D. Thesis, University of Minnesota.
29. Abragam, A., and Bleaney, B. (1970) *Electron Paramagnetic Resonance of Transition Metal Ions*, Oxford University Press, Oxford, U.K.
30. Percival, D. M., Denis, D., Riendeau, D., and Gresser, M. J. (1992) *Eur. J. Biochem. 210*, 109−117.
31. Newman, L. M., and Wackett, L. P. (1995) *Biochemistry 34*, 14066−14076.
32. Lipscomb, J. D. (1994) *Annu. Rev. Microbiol. 48*, 371−399.
33. Rosenzweig, A. C., Frederick, C. A., Lippard, S. J., and Nordlund, P. (1993) *Nature 366*, 537−543.
34. Sanders-Loehr, J. (1989) in *Binuclear Iron Center Proteins* (Loehr, T. M., Ed.) pp 375−466, VCH, New York.
35. Fox, B. G., Shanklin, J., Ai, J., Loehr, T. M., and Sanders-Loehr, J. (1994) *Biochemistry 33*, 12776−12786.
36. Fox, B. G., Shanklin, J., Somerville, C., and Münck, E. (1993) *Proc. Natl. Acad. Sci. U.S.A. 90*, 2486−2490.
37. Qian, H., Edlund, U., Powlowski, J., Shingler, V., and Sethson, I. (1997) *Biochemistry 36*, 495−504.
38. Green, J., and Dalton, H. (1985) *J. Biol. Chem. 260*, 15795−15801.
39. Liu, K. E., and Lippard, S. J. (1991) *J. Biol. Chem. 266*, 12836−12839.
40. Kazlauskaite, J., Hill, H. A., Wilkins, P. C., and Dalton, H. (1996) *Eur. J. Biochem. 241*, 552−556.
41. Liu, Y., Nesheim, J. C., Lee, S. K., and Lipscomb, J. D. (1995) *J. Biol. Chem. 270*, 24662−24665.
42. Atkin, C. L., Thelander, L., Reichard, P., and Lang, G. (1973) *J. Biol. Chem. 248*, 7464−7472.
43. Ravi, N., Prickril, B. C., Kurtz, D. M., Jr., and Huynh, B. H. (1993) *Biochemistry 32*, 8487−8491.
44. Kurtz, D. M. (1990) *Chem. Rev. 90*, 585−606.
45. Solomon, E. I., Brunold, T. C., Davis, M. I., Kemsley, J. N., Lee, S.-K., Lehnert, N., Neese, F., Skulan, A. J., Yang, Y.-S., and Zhou, J. (2000) *Chem. Rev. 100*, 235−350.
46. Shu, L., Broadwater, J. A., Achim, C., Fox, B. G., Münck, E., and Que, L., Jr. (1998) *J. Biol. Inorg. Chem. 3*, 392−400.
47. Liu, K. E., Valentine, A. M., Wang, D. L., Huynh, B. H., Edmondson, D. E., Salifoglou, A., and Lippard, S. J. (1995) *J. Am. Chem. Soc. 117*, 10174−10185.
48. Lindqvist, Y., Huang, W., Schneider, G., and Shanklin, J. (1996) *EMBO J. 15*, 4081−4092.

BI025901U